

RESEARCH

Open Access



The therapeutic effect of thermo-sensitive hydrogel loaded with recombinant mycobacterium smegmatis expressing exogenous IL-15 in abdominal metastasis

Qi Wang^{1†}, Yi Mei^{3†}, Wenmei Rao¹, Sen Hong¹, Aoxing Chen⁴, Yang Yang^{4,5*} and Qin Liu^{1,2,5*} 

Abstract

Background Tumor immunotherapy is one of the most promising strategies in cancer treatment. Specifically, intraperitoneal immunotherapy has emerged as a novel approach for dealing with abdominal metastases. Previously, we developed a genetically engineered strain of *Mycobacterium smegmatis* (Ms-IL15) that expresses the cytokine interleukin-15 (IL15), demonstrating significant anti-tumor effects after intratumoral injection. However, intratumoral infusion might not be feasible in the case of diffuse abdominal metastases, making intraperitoneal injection a preferred option.

Methods In this study, we developed a bacterial delivery system by incorporating Ms-IL15 into Poloxamer 407, an injectable thermosensitive hydrogel, for intraperitoneal administration. A murine model of peritoneal metastasis was established, and tumor-bearing mice were administered P407/Ms-IL15 once weekly for two consecutive weeks. The anti-tumor efficacy and alterations in the tumor immune microenvironment were systematically evaluated.

Results Intraperitoneal injection of this system exhibited a remarkable tumor-suppressive effect, significantly prolonging the survival of treated mice. Flow cytometric analysis of the tumor immune microenvironment revealed enhanced maturation and activation of dendritic cells (DC), an increased proportion of effector memory T cells and Granzyme B, and suppressed macrophage polarization towards the M2 phenotype.

Conclusions Our findings indicate that a hydrogel-based bacterial delivery system is a safe and effective approach for the treatment of abdominal metastases.

Keywords Abdominal metastases, Engineering bacteria, Poloxamer 407, Tumor immunotherapy, Tumor microenvironment

[†]Qi Wang and Yi Mei contributed equally to this work.

*Correspondence:

Yang Yang

wing_young7@hotmail.com

Qin Liu

liuqin@nju.edu.cn

Full list of author information is available at the end of the article



© The Author(s) 2025. **Open Access** This article is licensed under a Creative Commons Attribution-NonCommercial-NoDerivatives 4.0 International License, which permits any non-commercial use, sharing, distribution and reproduction in any medium or format, as long as you give appropriate credit to the original author(s) and the source, provide a link to the Creative Commons licence, and indicate if you modified the licensed material. You do not have permission under this licence to share adapted material derived from this article or parts of it. The images or other third party material in this article are included in the article's Creative Commons licence, unless indicated otherwise in a credit line to the material. If material is not included in the article's Creative Commons licence and your intended use is not permitted by statutory regulation or exceeds the permitted use, you will need to obtain permission directly from the copyright holder. To view a copy of this licence, visit <http://creativecommons.org/licenses/by-nc-nd/4.0/>.

Introduction

Peritoneal metastasis is a common complication in advanced colorectal cancer, affecting approximately 25% of patients as the disease progresses. This condition can result in severe complications such as abdominal pain, intestinal obstruction, and malignant ascites, significantly reducing patients' quality of life and worsening their prognosis. The five-year survival rate for patients with peritoneal metastasis remains below 10% [1, 2]. In patients with abdominal metastasis, traditional intravenous chemotherapy is restricted by dose-limiting toxicity, leading to insufficient drug concentration in the abdominal cavity and limited therapeutic efficacy [3, 4]. Compared with traditional intravenous or oral administration, regional intraperitoneal chemotherapy offers advantages such as higher drug concentrations in the peritoneal cavity, reduced systemic toxicity, and greater local anti-tumor efficacy, making it a focus of considerable attention in recent years [5]. Tumor treatment has entered a new era with immunotherapy; however, metastatic tumors create an immunosuppressive microenvironment, limiting the effectiveness of immunotherapy and preventing optimal outcomes [6]. An urgent challenge is to transform immune-desert tumors into inflammatory tumors to enhance the efficacy of immunotherapy.

Mycobacterium smegmatis (*M. smegmatis*) is a fast-growing, non-pathogenic saprophytic mycobacterium, renowned for its genetic stability and ease of manipulation. Its capacity to incorporate various heterologous genes efficiently renders it an ideal vaccine carrier [7]. Additionally, *M. smegmatis* has been demonstrated to activate dendritic cells, inducing CD8⁺ T cell-mediated immune responses and generating long-lasting memory T cells that contribute to anti-tumor activity [8]. Reports suggest that genetically engineered recombinant *Mycobacterium smegmatis* expressing tumor-associated antigens or cytokines has elicited significant anti-tumor immune responses in various mouse tumor models, including bladder and colorectal cancer [7, 9]. These discoveries emphasize the potential of *M. smegmatis* as a recombinant vaccine vector. Genetically modified *M. smegmatis* shows higher tumor-targeting specificity and reduced toxicity compared with the wild-type strain. The employment of appropriate adjuvants can further enhance the immunogenicity of the bacteria [10]. Interleukin-15 (IL-15) is a powerful immunostimulatory cytokine that promotes the proliferation and activation of T cells, natural killer (NK) cells, and dendritic cells (DCs), and also supports the persistence of CD8⁺ memory T cells, thereby activating the immune system [11].

However, in “naked drug” delivery, bacteria are prone to rapid metabolism and wide dissemination, making it challenging for them to accumulate at the tumor site for an extended period. This frequently necessitates

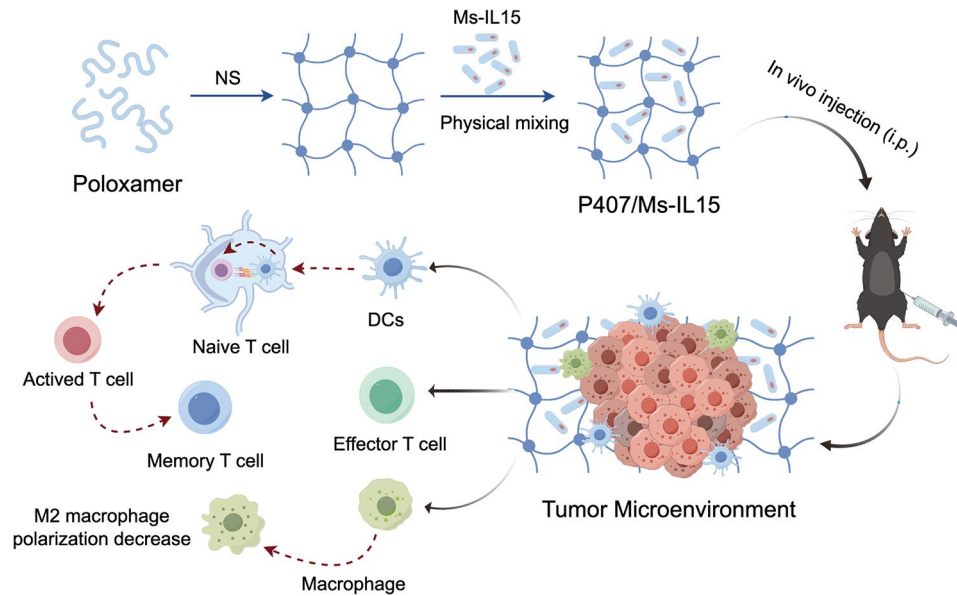
repeated administration or high doses to achieve the desired therapeutic effect, which may lead to additional adverse reactions [12]. Therefore, developing a safe and effective drug delivery system to enhance drug retention and utilization is of crucial importance. Injectable hydrogels have been extensively explored for therapeutic drug delivery [13]. Poloxamer 407 (P407), a U.S. Food and Drug Administration (FDA)-approved triblock copolymer composed of poly(ethylene oxide)-poly(propylene oxide)-poly(ethylene oxide) (EO-PO-EO), is biocompatible, injectable, and temperature-sensitive. At low temperatures, P407 is in a liquid state, but as the temperature rises, it gradually transforms into a stable gel state [14]. This gelled P407 can serve as a slow-release reservoir for drugs. Studies have demonstrated that Poloxamer-based in situ injectable hydrogels play a significant role in the delivery of anti-tumor drugs [15].

In this study, we have developed a cancer immunotherapy delivery system based on engineered *Mycobacterium smegmatis* (Ms-IL15) and the thermo-sensitive hydrogel Poloxamer 407. The in situ hydrogel P407 releases IL-15-expressing *M. smegmatis*, which promotes the maturation of dendritic cells (DCs), activates memory T cells and inhibits macrophage polarization towards the M2 phenotype (Scheme 1). Intraperitoneal injection of the P407/Ms-IL15 system enhances the local drug concentration, prolongs its action time, and effectively inhibits tumor growth. In conclusion, our findings present a therapeutic strategy for long-term tumor immunity mediated by engineered bacteria encapsulated in situ thermosensitive hydrogels, providing a promising approach for treating peritoneal metastases in advanced colorectal cancer.

Materials and methods

Materials, cells, bacterial strains, and animals

The Poloxamer 407 was purchased from BASF (P407/F127, Ludwigshafen, Germany). Ms-IL15 engineered bacteria strain, MC38 mouse colon cancer cell and H22 hepatocellular carcinoma cells were conserved by the Cancer Center of Nanjing Drum Tower Hospital Affiliated to the School of Medicine of Nanjing University. MC38 mouse colon cancer cell and H22 hepatocellular carcinoma cells were cultivated in Roswell Park Memorial Institute (RPMI) 1640 (Gibco) at 37°C and 5% CO₂, 10% fetal bovine serum, 100 U/ml penicillin, and 100 µg/ml streptomycin were added. The experimental animals were purchased from Shanghai Sippr-BK Laboratory Animal Co. Ltd. (Shanghai, China). All animals were raised in the Specific Pathogen Free (SPF) Laboratory Animal Center of Affiliated Nanjing Drum Tower Hospital of Nanjing University Medical School. All mice had unrestricted access to water and feed, and controlled ambient temperature (20–26°C), humidity (30–70%), and light/dark cycle (lights between 6 a.m. and 6 p.m.). All



Scheme 1 Schematic illustration of the preparation and mechanism of an injectable thermosensitive Poloxamer 407 hydrogel sustained-release system (P407/Ms-IL15) loaded with engineered *Mycobacterium smegmatis* (Ms-IL15). Intraperitoneal injection of P407/Ms-IL15 induces the maturation of dendritic cells (DCs), promotes the differentiation of memory T cells, and reduces macrophage polarization towards the M2 phenotype

animal experiments were sanctioned by the experimental Animal Ethics Committee of the Affiliated Nanjing Drum Tower Hospital of Nanjing University Medical School.

Preparation of P407 hydrogel

The P407 hydrogel was prepared through the “cold” method. For instance, to prepare a 20% poloxamer hydrogel solution, dissolve 1 gram of poloxamer powder in 5 mL of normal saline, and then stir at 4°C overnight until all particles are dissolved. Poloxamer solutions with concentrations ranging from 16 to 35% were prepared for preliminary analysis. When the solution becomes clear, Ms-IL15 is mixed and added to the gel.

Characteristic analysis of hydrogel

Place a 15 mL centrifuge tube in a 20°C or 37°C water bath, and use a 1 mL gun head to blow 1 mL hydrogel up and down until the gun head is blocked. The time taken for a fluid hydrogel to reach this point is referred to as the “gelation time”. Dynamic light scattering (DLS) measurements were carried out with a Malvern Zetasizer (Nano ZS, Malvern Ltd., UK). Solutions of 5% and 7.5% P407 were prepared, and the size, polydispersity index (PDI), and average particle size (Z-ave) were measured at 20°C. P407 hydrogel with 20% concentration was prepared, frozen at -80°C, vacuum dried, and then scanned by scanning electron microscope (SEM; SSX-550, SHIMADZU, Japan) observed its morphology. Cell Counting Kit 8 (CCK8) was employed to assess the cytotoxicity of P407 hydrogel against MC38 cells. Approximately 5×10^3 cells/pores were plated in a 96-well plate

containing RPMI 1640. After cell adhesion, RPMI 1640 was replaced with different concentrations of P407 hydrogel extracts (12.5%, 25%, 50%, 100%). All media were supplemented with 10% fetal bovine serum, 100 U/ml penicillin, and 100 µg/ml streptomycin. After incubation for 24, 48, and 72 h, RPMI 1640 medium mixed with CCK8 was added to the cells, with only the holes of the medium serving as a background measurement. After 2 h, the OD value of the sample at 490 nm was determined by a spectrophotometer (Thermo Scientific, USA). Cell survival rate calculation formula: Cell survival rate (%) = (treated cells - background) / (untreated cells - background) × 100.

Ms-IL15 release in vitro

1 mL of P407 hydrogel was mixed with 5×10^7 CFU of Ms-IL15 in a 15 mL centrifuge tube, stored at 37°C to induce gelation, and then 3 mL of 37°C PBS solution was spread on the gel. At the specified time points (0 h, 2 h, 4 h, 6 h, 8 h, 24 h, 48 h, 72 h and 96 h), 1 mL of sample was collected and 1 mL of 37°C PBS solution was added. The concentration of Ms-IL15 was determined at each time point, and the cumulative release was calculated as follows:

$$\text{Cumulative release(\%)} = \frac{C_n \times V_1 + \sum (C_{n-1} \times V)}{M} \times 100$$

C_n (CFU/mL): concentration of Ms-IL15 in the release solution at the Nth sampling; V_1 (mL): media-releasing total volume; V (mL): volume of the replacement solution; M (CFU): The total amount of Ms-IL15 in the hydrogel (5×10^7 CFU).

In vivo Ms-IL15 release

The in vivo release of Ms-IL15 in P407 hydrogel is detected through near-infrared imaging. Before intraperitoneal injection in MC38 mice, Ms-IL15 was stained with DIR (Bridgen, Beijing, China). DIR (5 μ M) was incubated with Ms-IL15 at room temperature for 30 min, then centrifuged (4500 rpm, 4°C, 10 min), and the precipitate was washed with NS three times to remove free dyes. Mice were intraperitoneally injected with DIR-stained Ms-IL15 or P407/ Ms-IL15 and then scanned at designated time points using the IVIS in vivo imaging system (PerkinElmer, Massachusetts, USA).

Establishment and treatment of abdominal metastasis tumor model

Male C57BL/6 mice aged 5–6 weeks were injected with 5×10^5 MC38 tumor cells into the right lower abdomen of each mouse. Seven days after tumor cell inoculation, the mice were randomly divided into 4 groups, with 5–6 mice in each group: NS (saline), P407 (hydrogel), Ms-IL15 (mycobacterium smegmatis), P407/Ms-IL15 (hydrogel-loaded mycobacterium smegmatis). Intraperitoneal injections of 5×10^7 CFU Ms-IL15 and 5×10^7 CFU P407/Ms-IL15 were dissolved in NS or 12% P407 at a final volume of 200 μ l each on day 7. One week later, the drug was administered again, twice. For dose-exploration experiments, different concentrations of P407/Ms-IL15 were intraperitoneally injected as described above. The weight of the mice was measured every 2–3 days for 3–4 weeks. The tumor load was monitored by IVIS on days 7, 14, and 21 after tumor vaccination. Before monitoring, 200 μ l of D-fluorescein with a concentration of 5 mg/mL was injected into the abdominal cavity of mice for fluorescence excitation. Mice were euthanized at the humane end once any of the following conditions were met: near death; weight loss or gain >20%; severe bloating. At the endpoint, the mice were euthanized and abdominal tumor nodules and abdominal effusion were collected to evaluate the immunotherapy effect of P407/Ms-IL15.

Establishment and treatment of malignant Ascites model

Male ICR mice aged 5–6 weeks were injected with 5×10^5 H22 tumor cells into the right lower abdomen of each mouse. After 7 days of tumor growth, randomly divide the mice into 4 groups ($n = 5-6$): NS (saline), P407 (hydrogel), Ms-IL15 (mycobacterium smegmatis), P407/Ms-IL15 (hydrogel-loaded mycobacterium smegmatis). On the 7th and 14th days, treat the ascites by intraperitoneal injection of 5×10^7 CFU Ms-IL15 and 5×10^7 CFU P407/Ms-IL15, respectively. These drugs were dissolved in NS or 12% concentration P407 hydrogel and the volume of each injection was 200 μ l per mouse. Measure the body weight, abdominal circumference and body temperature of the mice every 2–3 days for 20 days. After the

experiment, count the survival time, kill the mice, collect the peritoneal effusion and evaluate the tumor burden.

P407/Ms-IL15-induced immune response

Flow cytometry was utilized to detect the immune microenvironment alterations induced by P407/Ms-IL15. In the MC38 abdominal metastasized tumor model, mice in each group were sacrificed 7 days after the last administration (21 days after MC38 intestinal cancer cells were inoculated), and mesenteric lymph nodes and tumor tissues were removed. The single-cell suspension of mesenteric lymph nodes was prepared through the mechanical friction method. The tumor tissue was cut into small pieces, supplemented with collagenase type IV (1 mg/ml, Sigma), digested at 37°C for 2 h, and then filtered, lysed, and centrifuged to prepare a single-cell suspension. The activation of DC was detected with FITC anti-mouse CD11c antibodies, PE anti-mouse CD86 antibodies, and APC anti-mouse CD80 antibodies. The TCM and TEM of lymph nodes and tumor tissues were identified through FITC anti-mouse CD3 antibody, PE anti-mouse CD44 antibody, PerCP/Cy5.5 anti-mouse CD8 antibody, and APC anti-mouse CD62L antibody. PE/Cy7 anti-mouse GZMB antibody were used as markers of Granzyme B. FITC anti-mouse CD11b antibody and PE/Cy5 anti-mouse F4/80 antibody were employed to identify macrophages, and PE anti-mouse CD86 antibody and BV421 anti-mouse CD163 antibody were used as markers of M1 and M2 macrophages. All antibodies were purchased from Biolegend, USA. All single-cell suspensions were stained at 4°C in the dark, incubated for 30 min, and washed with PBS three times before detection. Cells were collected using Beckman CytoFLEX (Beckman, USA) and analyzed by FlowJo software.

Safety analysis

The mice in each group were sacrificed on the 14th day after the last administration. The heart, liver, spleen, lungs, kidneys, and other abdominal organs were removed, fixed with 4% formaldehyde, then made into 4 μ m thick paraffin-embedded sections, stained with hematoxylin-eosin, and histological analysis was conducted under the optical microscope (DM5000, Leica, Germany). Additionally, serum was collected on the 14th day after the last dose, and liver and kidney function was determined by measuring the levels of alanine aminotransferase, aspartate aminotransferase, alkaline phosphatase, creatinine, and urea. Perform a comprehensive blood cell count by quantifying white blood cells, red blood cells, hemoglobin levels, and platelet counts. The test was performed in the Laboratory of Nanjing Drum Tower Hospital Affiliated to the School of Medicine of Nanjing University.

Statistical analysis

Statistical analysis was completed through GraphPad Prism 9.4.1. All results are presented as mean \pm SEM for at least three independent experiments. For antitumor studies, there were 5–7 mice in each group. P-values were calculated by two-tailed unpaired Student's t-tests. $P < 0.05$ was considered as with statistical significance ($^{ns}p > 0.05$, $^{*}p < 0.05$, $^{**}p < 0.01$, $^{***}p < 0.001$ and $^{****}p < 0.0001$). Animal survival was presented using Kaplan-Meier survival curves and was statistically analyzed using a log-rank test. All image typesetting was accomplished in Adobe Illustrator.

Results

Preparation and characterization of P407/Ms-IL15

The results show that the gelation kinetics time of poloxamer 407 depends on the concentration and temperature. To better package Ms-IL15 into the P407, we need to consider the size and release capacity of the gelated micelles. Therefore, the gelation time of P407 hydrogel at different concentrations was measured at room temperature (20°C) and body temperature (37°C). The results showed that 16% P407 could not form glue at room temperature and 37°C. The hydrogel at 25% concentration had a gel time of 260 s at room temperature (RT), while the P407 at 30% and 35% concentration had the disadvantage of gelating too quickly at room temperature, at 155 and 135 s, respectively (Fig. 1A). With the increase of concentration of P407 at 37°C, the gelation time was significantly shortened, which was 63 s for 20%, 42 s for 25%, 30 s for 30%, and 23 s for 35% (Fig. 1B). It is worth noting that a 20% concentration of hydrogel can only achieve sol-gel transformation at physiological temperature, and there is enough injection time at room temperature, which may be the appropriate concentration for our administration of Ms-IL15. However, considering the potential damage caused by the adhesion of P407 to normal organs after intraperitoneal injection, we will use 12% concentration of hydrogel for subsequent in vivo experiments. The addition of Ms-IL15 at room and body temperature did not affect the gelation time (Fig. 1C and D). In order to visualize the change of P407 sol to gel, methylene blue dye was added and observed by the inversion method. As shown in Fig. 1E, P407 hydrogel (20%) has good fluidity at room temperature, and sol-gel transformation occurs when the temperature rises to 37°C. Mixed P407/Ms-IL15 hydrogel (5×10^7 CFU Ms-IL15 and 20% P407) has similar state.

P407 can self-assemble into microclumps due to its amphiphilicity in water. As measured by dynamic light scattering (DLS), P407 microclusters have formed at concentrations of 5% and 7.5%. Figure 1F depicts the representative size distribution of microclusters at 5%P407. As shown in Fig. 1G and H, the average Z-ave and PDL of

P407 at 5% concentration are 26.34 nm and 0.346 nm, and for 7.5% concentration, Z-ave and PDL are 31.23 nm and 0.484 nm, respectively. The scanning electron microscope (SEM) images showed that the blank P407 hydrogel had a rich porous channel-like structure from 150 \times magnifications (Fig. 1I). After loading Ms-IL15 and magnifying by 2000 times, it can be observed that Ms-IL15 attached to the hydrogel porous structure (Fig. 1J). Furthermore, the porous channel structure of the P407/Ms-IL15 hydrogel (20%) is analogous to that of the blank hydrogel (Fig. 1K), which is consistent with previous reports [15, 16].

Ms-IL15 release from poloxamer 407 hydrogel in vitro and vivo

We first studied the release of Ms-IL15 in P407 hydrogel (20% concentration) in vitro. As shown in Fig. 2A, the P407 hydrogel was explosively released at the initial stage, with about 70% of the Ms-IL15 load released within 24 h, and Ms-IL15 was completely released from the P407 hydrogel after 96 h. Overall, our P407/Ms-IL15 hydrogel was sustainably released in vitro for up to 4 days, which is consistent with the degradation of the P407 hydrogel (Fig. 2B). Next, we studied the release of Ms-IL15 in mice. In our design, Ms-IL15 is mixed with the P407 hydrogel (12%) before it is gelated so that it is evenly distributed in the micelle at room temperature. When exposed to body temperature, the P407 hydrogel rapidly transforms into a gel state loaded with Ms-IL15, which favors the bacteria to remain stable in the hydrogel for a long time. To visualize the slow release of Ms-IL15 from P407 hydrogel, DIR-stained Ms-IL15 coated with P407 hydrogel was intraperitoneally injected using near-infrared fluorescence imaging (NIR). As shown in Fig. 2C and D, Ms-IL15 in both groups showed an initial growth trend after intraperitoneal injection and began to decline after reaching its peak growth. For the pure Ms-IL15 group, the fluorescence disappeared 28 days after injection, indicating that Ms-IL15 was eliminated, while the peak value of the P407/Ms-IL15 group was much higher than that of Ms-IL15 group, and fluorescence was still present 28 days after injection, but not eliminated, indicating that P407 hydrogel could increase the amount of Ms-IL15 retained in the body. At the same time, the release and consumption time are prolonged, and the long-lasting anti-tumor effect is played.

To ensure that the P407 hydrogel was well tolerated, we tested it in the MC38 cell line (Fig. 2E). MC38 cells were incubated with different concentrations of P407 and cell viability was assessed with CCK-8. For any concentration of P407 hydrogel, cell viability in the MC38 cell line did not decrease with time. Our data suggest that P407 is biocompatible and does not produce tumor-killing effects on its own, which is consistent with previous findings in the literature [15].

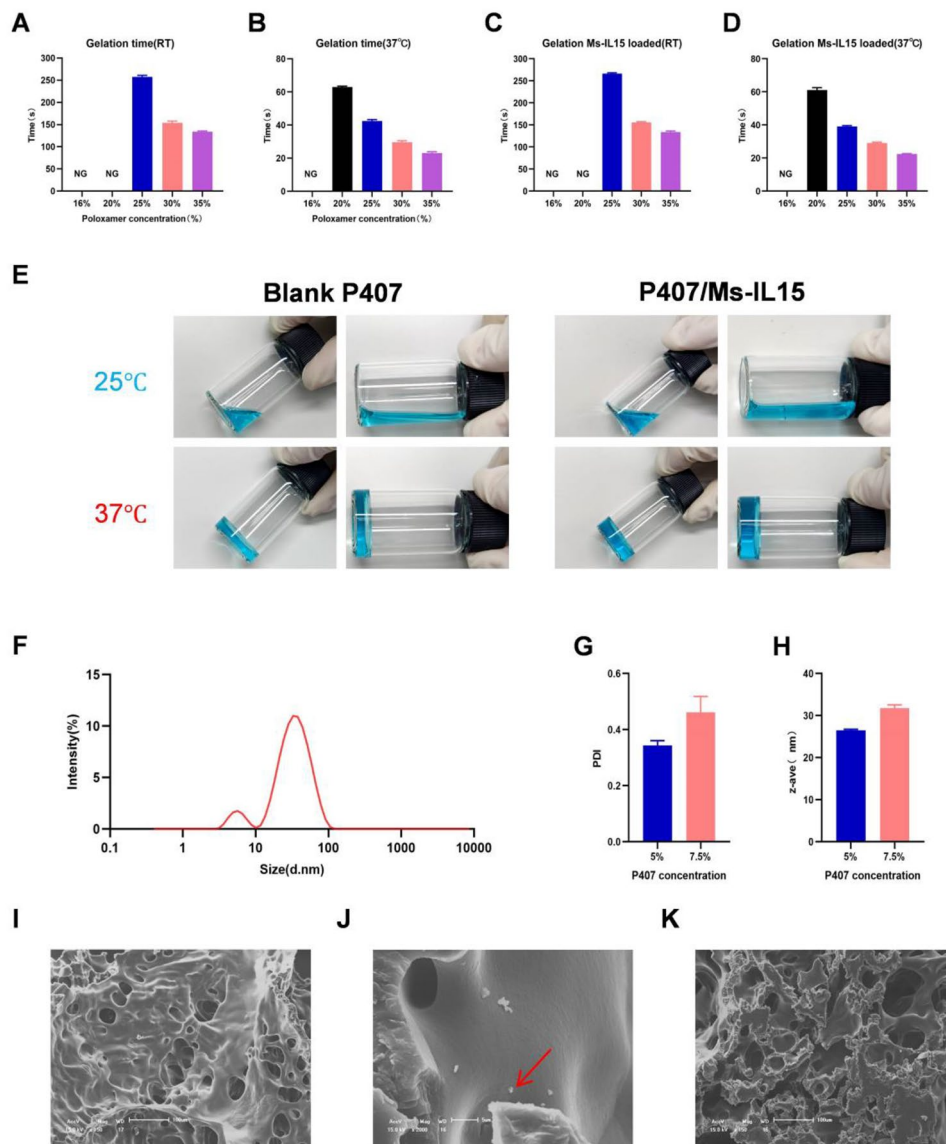


Fig. 1 Preparation and characterization of poloxamer 407 hydrogel. **A-D**, Time to gelation under different conditions. **A**, Blank P407 gel at room temperature; **B**, Blank P407 gel at 37°C; **C**, P407 hydrogel loaded with Ms-IL15 at room temperature; **D**, P407 hydrogel loaded with Ms-IL15 at 37°C; **E**, The reversible sol-gel phase transition between blank P407 hydrogel and P407/Ms-IL15 at 25 to 37°C. **F**, The representative histogram of the micelle (5%) obtained by dynamic light scattering; **F-H**, The PDI and average size (z-ave) of the hydrogel micelle. **I**, Scanning electron microscope images of blank P407 hydrogel (20 wt%, scale bar is 100 μ m). **J**, Representative images of Ms-IL15 in P407 hydrogel (Manifested by the arrows, the scale bar is 5 μ m). **K**, P407 hydrogel loaded with Ms-IL15, Ms-IL15 loading amount: 5×10^7 CFU mL⁻¹

Determination of concentration of Ms-IL15 encapsulated by P407 hydrogel

To determine the concentration of Ms-IL15 encapsulated in the P407 hydrogel, we examined the dose-effect relationship using a peritoneal transfer model. First, the peritoneal metastasis model was formed by intraperitoneal inoculation of 5×10^5 MC38 mouse colon tumor cells into C57BL/6 male mice aged 5–6 weeks, and the mice were randomly divided into 4 groups 7 days after inoculation. In addition, four different concentrations of Ms-IL15 (including 0, 1×10^6 CFU, 1×10^7 CFU, and 5×10^7 CFU) were dissolved in 12% P407 for

intraperitoneal injection within 2 weeks (Fig. 3A), and the drug was administered twice in total (Fig. 3A). The tumor size was monitored by a near-infrared imaging system (IVIS) every 5–7 days. IVIS evaluation of the treatment effect showed that tumor development was significantly inhibited in the 5×10^7 CFU Ms-IL15 group (Figs. 3B and C). At the end of treatment, tumor nodule weight and ascites volume in the 5×10^7 CFU group had the best inhibition effect (Fig. 3D-F). There was no significant difference in body weight among the four groups of mice (Fig. 3G). Considering the above

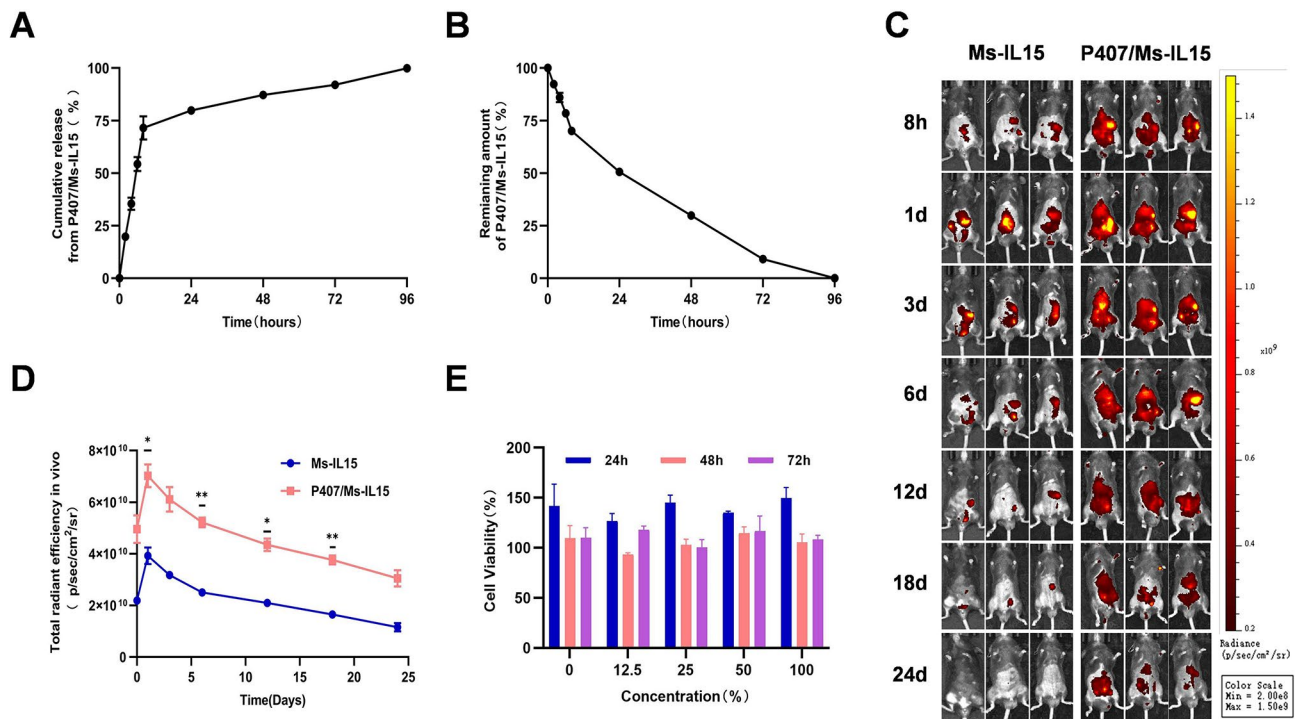


Fig. 2 Release of Ms-IL15 from the P407 hydrogel both in vivo and in vitro **A**, Ms-IL15 release from 20% P407 hydrogel. Ms-IL15 loading amount: 5×10^7 CFU/mL. The error bars mean \pm SEM for 3 independent experiments, $n=3$ respectively; **B**, Degradation of Ms-IL15 loaded 20% P407 hydrogel in A; **C**, Near-infrared (NIR) imaging of male C57BL/6 mice on 8 h, 1 day, 3 days, 6 days, 12 days, 18 days, and 24 days after intraperitoneal injection of Ms-IL15 (5×10^7 CFU in 200 μ l normal saline) or P407/Ms-IL15 (5×10^7 CFU in 200 μ l 12% P407 solution) ($n=3$). Ahead of injection, Ms-IL15 was dyed with DIR (5 μ M); **D**, Change of total fluorescence flux over time after injection of Ms-IL15 or P407/Ms-IL15 in C57BL/6 mice. The error bars represented mean \pm SEM; **E**, MC38 cells were cultured with different concentrations of P407 for 24 h, 48 h, and 72 h. At indicated time points, a CCK8 kit was added and the change in optical density of the formed product was measured at 490 nm. Error bars represented mean \pm SEM ($n=3$)

experimental results, we finally selected 5×10^7 CFU Ms-IL15 to treat mice.

Antitumor effect of P407/Ms-IL15 in abdominal metastasis model

After determining the optimal concentration for intraperitoneal injection of P407/Ms-IL15, we further tested the antitumor efficacy of the P407/Ms-IL15 hydrogel delivery system in a mouse model of intraperitoneal metastases. To establish a model of intraperitoneal metastasis, 5×10^5 MC38 mouse colonic tumor cells were intraperitoneally inoculated into 5–6 week-old C57BL/6 male mice on day 0. We randomly divided the mice into four groups: NS, P407, Ms-IL15, and P407/Ms-IL15, which were administered twice every 7 days (Fig. 4A). On day 21 of tumor vaccination, we found a significant reduction in tumor nodules in the abdominal cavity in the P407/Ms-IL15 group. We then euthanized the mice on day 7 after the last dose, collected tumor tissue, and weighed it. Tumor tissue from the NS and P407 groups was similar in volume and larger than the other 2 groups (Fig. 4B). The weight of tumor tissue (345.1 g) in the P407/Ms-IL15

group was nearly 8 times lower (2515 g and 2553 g) than in the NS and P407 groups (Fig. 4C). Nir imaging results showed that the bioluminescence range in the abdominal cavity of the NS group gradually increased with time, while the P407/Ms-IL15 group was almost undetectable on day 14, indicating that P407/Ms-IL15 could effectively inhibit the development of abdominal metastasized tumors (Fig. 4D and F). As shown in Fig. 4E, the body weight of mice in the P407/Ms-IL15 group decreased to a lesser extent, with no significant difference compared to the NS group. However, the body weight of mice in the Ms-IL15 alone group decreased more significantly. The sustained-release effect of P407 alleviated the potentially latent toxicity of Ms-IL15. For the study of survival, all mice in the P407/Ms-IL15 group survived to the endpoint of monitored treatment, while 60% of mice in the Ms-IL15 group died before 60 days, compared to a median survival of less than 30 days in the control group treated with NS and P407 (Figs. 4G). Overall, these studies suggest that the slow-release ability of P407 hydrogel and its adhesion to abdominal metastases further enhance the tumor suppressive effect of Ms-IL15.

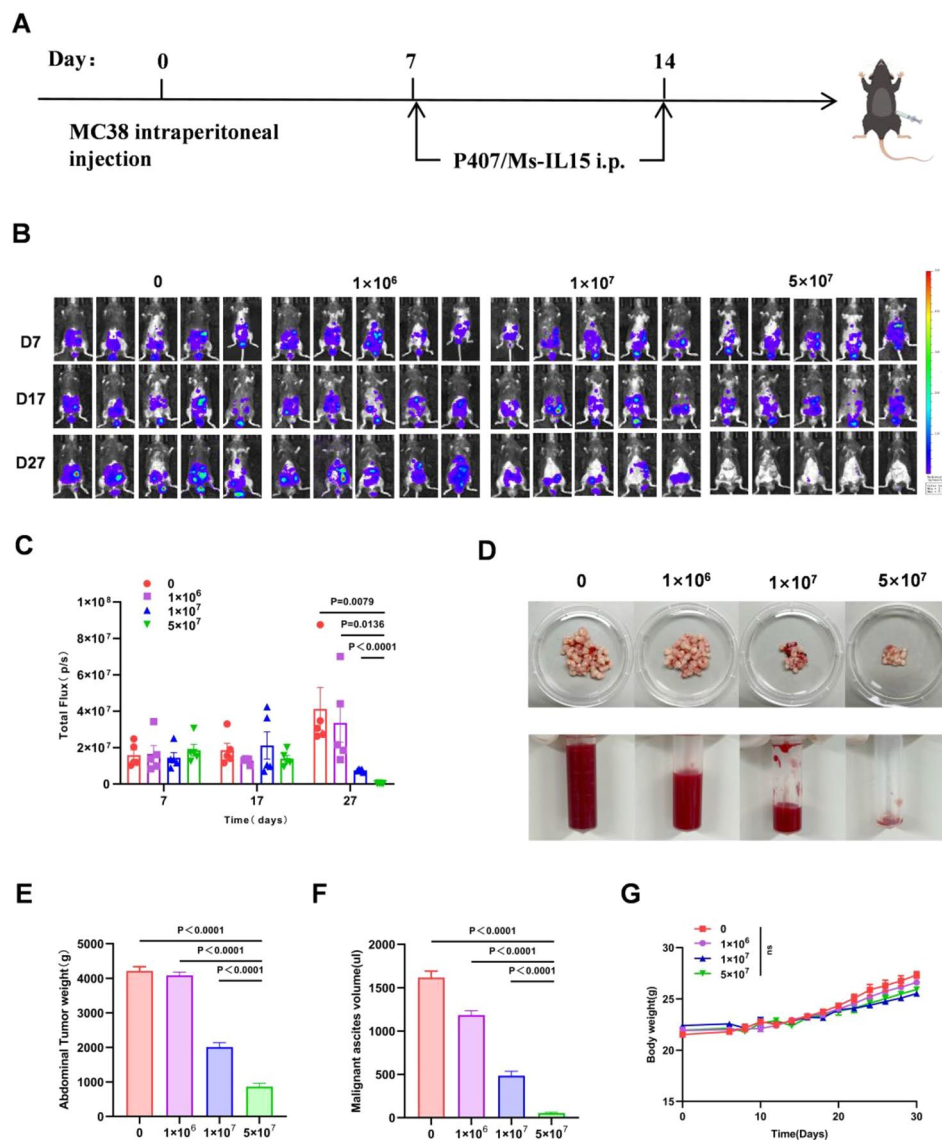


Fig. 3 Optimal dose for intraperitoneal injection of P407/Ms-IL15. **A** Schematic diagram of administration of P407/Ms-IL15 in MC38 tumor-bearing mice. 5×10^5 cells were injected subcutaneously on the right lower sides of the abdomen to establish the MC38 tumor model. The mice were injected intraperitoneally with P407, 1×10^6 P407/Ms-IL15, 1×10^7 P407/Ms-IL15 or 5×10^7 P407/Ms-IL15 which were dissolved a final volume of 200 μ l per dose 7 days after inoculation. P407 concentration was 12%. The body weight was measured every 2–3 days to termination. **B**, Intraperitoneal tumor burden monitored with IVIS of mice with the indicated treatment on Day 7, Day 17, Day 27. **C**, Bioluminescence intensity in the region of interest (ROI) within the abdominal area ($n=5$). **D**, Representative photographs of abdominal tumors and ascites harvested from mice in each group. **E**, Average abdominal tumor weight of different groups. **F**, Average abdominal tumor weight of different groups. **G**, The average body weight of different groups ($n=5$). For the analysis in C and E–F, error bars represented mean \pm SEM ($n=5$). Statistical significance was determined by analysis of two-tailed unpaired Student's *t*-tests. ns represented $p > 0.05$

Immune response induced in vivo by the P407/Ms-IL15 hydrogel system

In order to further understand the mechanism by which P407/Ms-IL15 in-situ hydrogel induced immune response in the abdominal cavity, we repeated the above tumor suppression experiment. Abdominal tumor tissues and mesenteric lymph nodes were harvested on the 7th day after the last administration, and the changes in immune population were detected by flow cytometry, as

shown in Figs. 5A–G, Figure S1A–C, and Figure S2A–E. The proportion of activated DC from tumor tissue increased in both Ms-IL15 and P407/Ms-IL15 groups, with the highest in the P407/Ms-IL15 group, which increased by about 2.8 times compared with the NS group (Fig. 5C). The proportion of effector memory T cells (TEM) that play an important role in killing tumor cells was then measured, and results showed that P407/Ms-IL15 (74.77%) had higher TEM infiltration compared

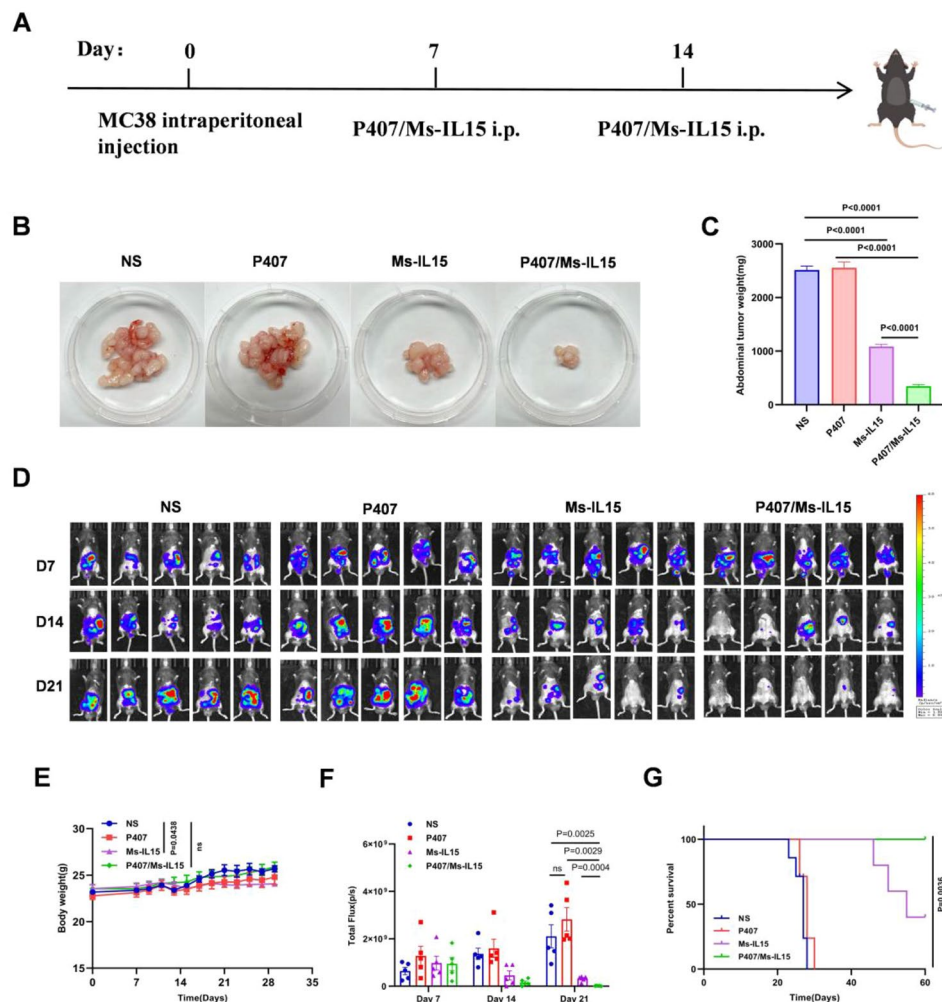


Fig. 4 P407/Ms-IL15 can effectively inhibit the development of abdominal metastases. **A** Schematic diagram of P407/Ms-IL15 in the treatment of MC38 colon cancer with peritoneal metastasis. C57BL/6 mice were intraperitoneally inoculated with MC38 cells (5×10^5 per mouse) and randomized into four groups with intraperitoneal treated with NS, P407, Ms-IL15, P407/Ms-IL15 on Days 7 and 14. **B**, Representative abdominal tumor nodules were harvested 7 days after the last treatment in different groups of mice. **C**, Average abdominal tumor weight in different groups of mice ($n=5$). **D**, Near infrared fluorescence imaging of mice at day 7, 14, and 21 in different treatment groups ($n=5$). **E**, The average weight of the different groups ($n=5$). **F**, Tumor burden represented by total flux (photons s^{-1}) plotted on indicated times. **G**, Survival curves of different groups for 60 days ($n=5$). Data were the mean \pm SEM. For the analysis in **C** and **E-F**, statistical significance was determined by analysis of two-tailed unpaired Student's *t*-tests. Differences in survival were determined by using the Kaplan–Meier method, and the *p*-value was determined via the log-rank (Mantel-Cox) test. ns represented $p > 0.05$

to Ms-IL15 (63.52%) and the other groups (Fig. 5E). Furthermore, P407/Ms-IL15 enhanced the expression of granzyme B (GZMB), a key cytotoxic protein, in CD8 + T cells within the tumor tissue (Fig. 5G). In addition, we investigated the proportion of tumor-associated macrophages (Tams), which are an important component of the innate immune system, and we found that P407/Ms-IL15 reduced the proportion of immunosuppressive type 2 macrophages (Fig. 5F). In addition, the immune subpopulations of mesenteric lymph nodes also changed after peritoneal administration of P407/Ms-IL15, as shown in Fig. 5B and D, and Figure S1C. P407/Ms-IL15 can cause a significant increase in mature DC cells and effector memory T cells in mesenteric lymph nodes, along

with enhanced granzyme B expression in CD8 + T cells. Together, these data suggest that intraperitoneal injection of P407/Ms-IL15 in situ hydrogel can activate both innate and adaptive immune responses, thereby reprogramming the immune microenvironment of mice with abdominal metastases and further improving the immune effects of Ms-IL15.

P407/Ms-IL15 complex effectively suppresses the development of malignant Ascites

To comprehensively assess the anti-tumor efficacy of the P407/Ms-IL15 hydrogel delivery system, we conducted an experimental validation using a mouse model of hepatocellular carcinoma with malignant ascites. On day

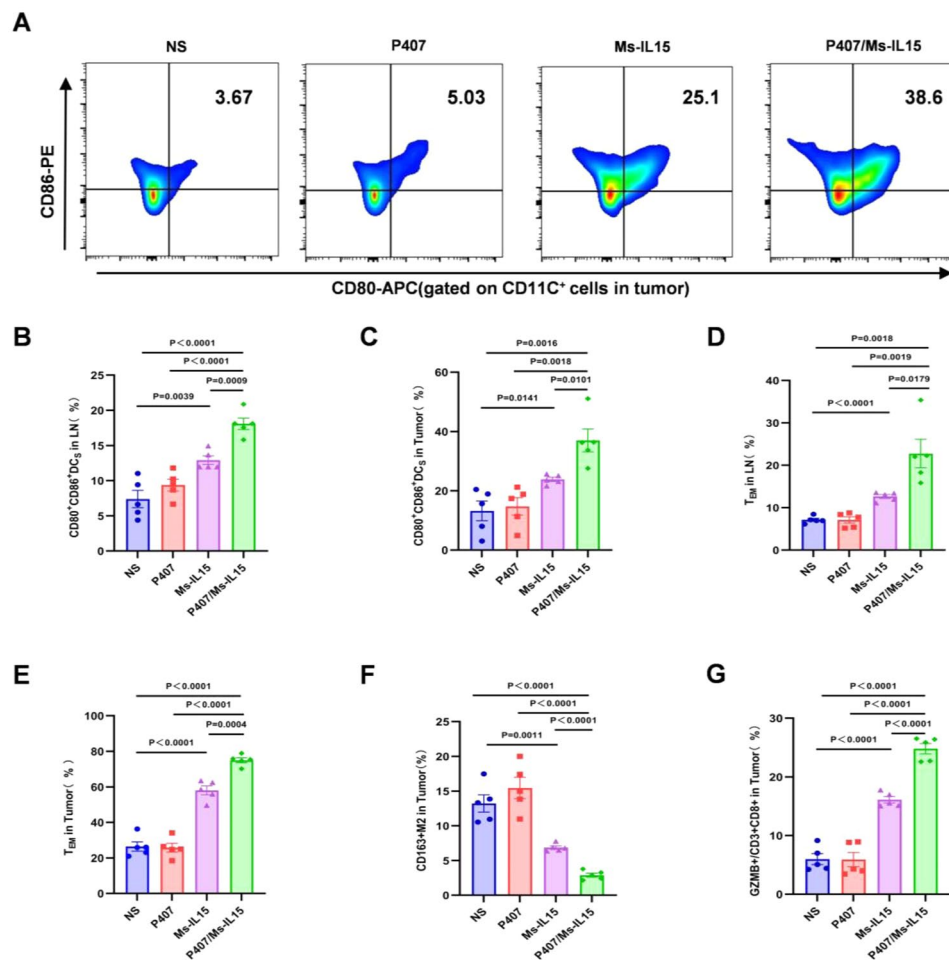


Fig. 5 P407/Ms-IL15 further reprograms the immune microenvironment in vivo. Different groups of MC38 tumor-bearing mice were euthanized 7 days after the last treatment, and the proportion of immune cells in abdominal tumors and mesenteric lymph nodes ($n=5$) was analyzed by staining and flow cytometry. **A**, Representative flow diagram of CD11c⁺CD80⁺CD86⁺DCs in tumor tissue. **B**, The proportion of CD11c⁺CD80⁺CD86⁺DCs in mesenteric lymph nodes. **C**, The proportion of CD11c⁺CD80⁺CD86⁺DCs in tumor tissue. **D**, The proportion of effector memory T cells (TEM, CD3⁺CD8⁺CD44⁺CD62L⁻) in mesenteric lymph nodes; **E**, The proportion of effector memory T cells (TEM, CD3⁺CD8⁺CD44⁺CD62L⁻) in tumor tissue. **F**, The proportion of M2-type macrophages in tumor tissues (F4/80⁺CD11b⁺CD163⁺). **G**, The proportion of granzyme B in CD8⁺T cells in tumor. ns represented $p > 0.05$

0.5×10^5 H22 murine hepatocellular carcinoma cells were intraperitoneally inoculated into male ICR mice aged 5–6 weeks. On day 7 post-inoculation, the mice were randomly assigned to four treatment groups: NS, P407, Ms-IL15, and P407/Ms-IL15. Intraperitoneal administration was performed twice at 7-day intervals (Fig. 6A). By day 21 post-inoculation, we observed that the body weight (Fig. 6C) and abdominal circumference (Fig. 6D) of mice in the P407/Ms-IL15 group were significantly lower than those in the other three groups, indicating that P407/Ms-IL15 effectively suppressed the development of malignant ascites. During the treatment period, no significant changes in body temperature were noted across all groups, and the differences were not statistically significant (Fig. 6E), suggesting that the treatment did not induce toxic side effects. On day 7 following the final administration, peritoneal effusion was collected from

the mice and its volume was measured. The volumes of malignant ascites in the NS and P407 groups were similar and markedly higher than those in the Ms-IL15 and P407/Ms-IL15 groups (Fig. 6F). Specifically, the volume of malignant ascites in the P407/Ms-IL15 group (3512 ul) was approximately 2.5 times smaller than that in the NS (8606 ul) and P407 (8770 ul) groups (Fig. 6G). In the survival analysis, all mice in the P407/Ms-IL15 group survived for more than 30 days, whereas the median survival time of mice in the Ms-IL15 group was 27 days. In contrast, the median survival time of mice in the control groups treated with NS and P407 was less than 25 days (Fig. 6B). Collectively, these findings demonstrate that the P407/Ms-IL15 hydrogel delivery system effectively inhibits the progression of malignant ascites in mice and exhibits potent anti-tumor activity.

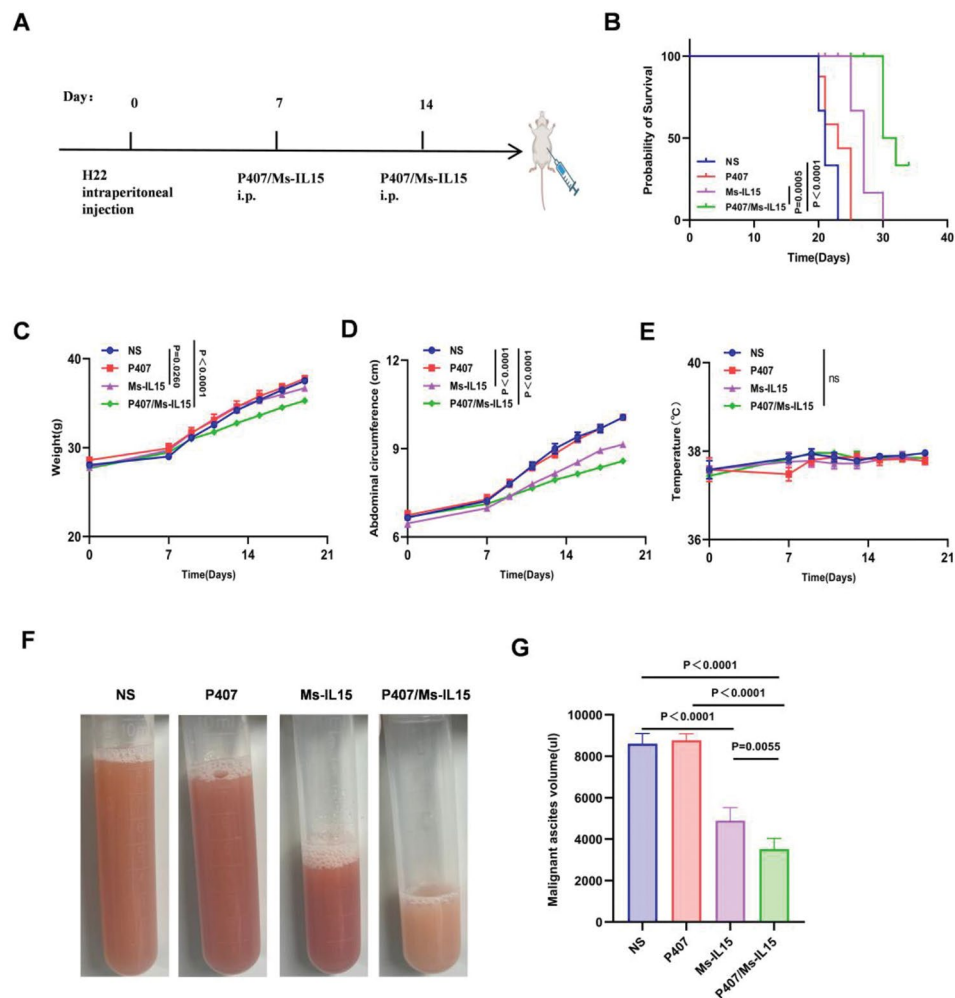


Fig. 6 Efficacy of Different Treatments in a Mouse Model of Malignant Ascites from Hepatocellular Carcinoma. **A**, Schematic representation of the P407/Ms-IL15 treatment regimen in an H22 hepatocellular carcinoma mouse model with malignant ascites; **B**, Survival curves of different groups over 35 days; **C**, Average weight changes across different groups; **D**, Average changes in abdominal circumference among different groups; **E**, Average body temperature changes in different groups; **F**, Representative images of visible malignant ascites collected from different groups 7 days after the final treatment; **G**, Average volume of malignant ascites in different groups ($ns\ p > 0.05$)

Biosafety assessment of intraperitoneal vaccination with P407/Ms-IL15

For better clinical application, it is necessary to evaluate the biosafety of P407/Ms-IL15. For in vivo experiments, mice in the Ms-IL15 group alone lost weight over time during treatment, and mice in the P407/Ms-IL15 group lost less weight due to in situ sustained release and barrier effects (Fig. 4E). We believe that large bursts of Ms-IL15 in a short period of time resulted in weight loss compared to the P407/Ms-IL15 group. In addition, changes in major organs of mice in each group were detected 7 days after the last administration, and hematoxylin-eosin staining was performed on the heart, liver, spleen, lungs, and kidneys of mice from different groups, and no significant pathological changes were observed (Fig. 7A). Furthermore, we performed pathological evaluations of the abdominal organs potentially affected by intraperitoneal

injection (including the bladder, intestines, and testes), and no evidence of organ damage was observed (Figure S3). These findings further substantiate the safety profile of the P407/Ms-IL15 hydrogel delivery system. Peripheral blood was collected from the mice for assessment of liver and kidney function, as well as routine hematological analysis. No significant alterations were observed in serum levels of alanine aminotransferase (ALT), aspartate aminotransferase (AST), alkaline phosphatase (ALP), urea (UREA), creatinine (CREA), red blood cells (RBC), white blood cells (WBC), hemoglobin (HGB) and platelets (PLT) of mice in all groups, and they were basically at the same level, with no statistical significance (Fig. 7B-C). In summary, in situ injection of thermosensitive P407 hydrogel has good biosafety.

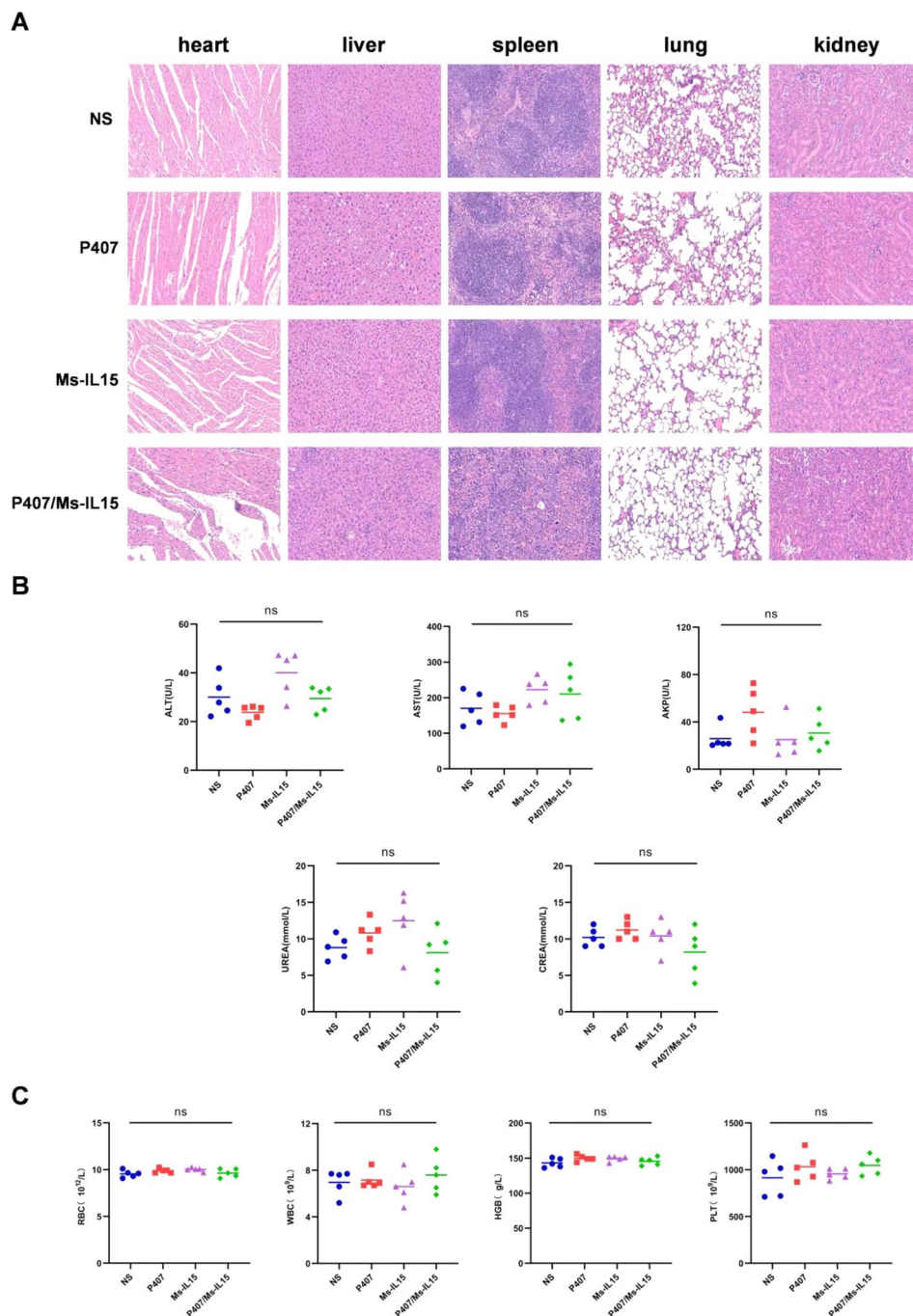


Fig. 7 Biosafety assessment of intraperitoneal inoculation of P407/Ms-IL15. **A**, Fourteen days days after the last treatment ($n=5$), the hearts, livers, spleens, lungs, and kidneys of tumor-bearing mice were stained with hematoxylin-eosin. The scale is 200 μ m. **B**, The index of blood liver and kidney function in mice. ALT, alanine aminotransferase; AST, glutamic oxalacetic transaminase; AKP, alkaline phosphatase; CREA, creatinine; UREA, hematuria nitrogen. **C**, The blood count tests in mice. RBC, red blood cell; WBC, white blood cell; HGB, hemoglobin; PLT, Platelets

Discussion

In recent years, immunotherapy has offered new hope for patients with peritoneal metastases. Several preclinical studies and clinical trials have demonstrated that intraperitoneal injection of immune drugs can induce tumor regression in both mice and humans [17, 18].

Nevertheless, the immunosuppressive microenvironment of the peritoneum constrains the efficacy of these therapies, and finding means to activate a more effective immune response remains an urgent challenge. The utilization of microorganisms in tumor therapy has emerged as a field of significant interest, playing a crucial role in

reprogramming the tumor immune microenvironment [19, 20]. BCG (Bacillus Calmette-Guérin), an attenuated strain derived from mycobacterium bovis, has been approved by the FDA for the treatment of non-muscle-invasive bladder cancer [21]. Mycobacterium smegmatis, a non-pathogenic microorganism within the mycobacterium genus, serves as an ideal delivery vector akin to BCG (Bacillus Calmette-Guérin). Additionally, compared with BCG, mycobacterium smegmatis exhibits greater susceptibility to damage inflicted by phagolysosomal proteases within the phagocytic vesicles of infected cells. This enhances the release of therapeutic agents, subsequently activating dendritic cells and inducing CD8 + T cell-mediated immune responses, leading to the generation of long-lasting memory T cells [8, 22]. Due to its remarkable safety and practicability, Mycobacterium smegmatis shows a promising potential as an immunomodulator in the field of anti-tumor drug research [23]. Engineered Mycobacterium smegmatis, which expresses cytokines or tumor-associated antigens, exerts strong anti-tumor effects in various mouse models of tumors such as bladder cancer by activating DCs and eliciting CD8 + T cell-mediated immune responses [7, 9, 24]. Our team previously engineered Mycobacterium smegmatis expressing IL15 to stimulate tumor-specific immune responses through intratumoral injection. However, the feasibility of this therapy is limited in metastatic tumors lacking a primary focus. To address this issue, we believe that local abdominal administration is a favorable option, as it increases the concentration of drugs at the disease site while reducing the risk of systemic side effects.

With the continuous advancement of materials science, hydrogels have been developed for bacteria-mediated diagnosis and treatment, such as the utilization of bacteria to diagnose intestinal inflammation or promote wound healing [15, 25]. In tumor treatment, bioluminescent Salmonella typhimurium encapsulated in a sodium alginate-based hydrogel, along with the photosensitizer dihydroporphyrin e6 (Ce6), has exhibited effective tumor growth inhibition [26]. Additionally, chitosan-sodium alginate hydrogels loaded with engineered bacteria can activate both intestinal mucosal and systemic immunity, suppressing tumor growth [27]. Poloxamer 407 (P407), a temperature-sensitive injectable hydrogel, has been demonstrated in our study to maintain its structural integrity when combined with bacteria, consistent with previous reports [28]. P407 also supports bacterial growth and prolongs bacterial residence at the injection site without influencing bacterial secretion [29]. We hypothesize that P407 can slow the metabolism of Ms-IL15 in the body, enhancing its anti-tumor effect. Based on these findings, we have developed a P407/Ms-IL15 thermosensitive hydrogel drug delivery system, which can be administered intraperitoneally to significantly inhibit tumor

growth in the long term. This effect is primarily attributed to the temperature sensitivity, excellent adhesion, and sustained release properties of the P407 hydrogel.

In our study, the P407/Ms-IL15 treatment elicited an anti-tumor immune response through the interactions among T cells, dendritic cells (DCs), and macrophages. Flow cytometry analysis revealed an increased proportion of dendritic cells (DCs) and memory T cells in both tumor tissues and mesenteric lymph nodes. Additionally, a higher percentage of CD8 + T cells expressed granzyme B, which is known for its cytotoxic effects on tumor cells. Concurrently, there was a reduction in the number of immunosuppressive M2-polarized macrophages. Furthermore, no significant differences were observed in body weight, body temperature, liver and kidney function, complete blood cell count, or vital organ status between P407/Ms-IL15-treated mice and the control group. These findings suggest that local hydrogel injection exhibits excellent safety. More importantly, this drug delivery strategy overcame the challenges of systemic drug administration, enhancing drug retention at the abdominal lesion site and tumor microenvironment, thereby maximizing the activation of immune cells and strengthening the therapeutic effect of Ms-IL15. Meanwhile, it also offers a promising therapeutic strategy for the management of patients with abdominal metastatic tumors in clinical settings.

Despite the promising outcomes, our study has certain limitations. For instance, further exploration of the biological distribution of P407/Ms-IL15 in mice would offer deeper insights into the tumor-targeting ability of the bacteria and the role of the hydrogel in this system. Notably, the concentration of P407 used for intraperitoneal injection differed from that used *in vitro*. This was mainly to avoid potential damage, as a high concentration of P407 could adhere to normal organs, such as the intestines, after intraperitoneal injection. Another limitation is that we only evaluated the anti-tumor effects of P407/Ms-IL15 in two tumor models, which restricts the universality of the findings. We plan to assess the anti-tumor effects of P407/Ms-IL15 in other tumor models to confirm its broader applicability. Additionally, exploring the synergistic effects of P407/Ms-IL15 with radiotherapy, chemotherapy, immune checkpoint inhibitors, and other therapies is an important direction for future research.

Conclusion

In summary, this study successfully developed an injectable thermosensitive hydrogel delivery system loaded with engineered Mycobacterium smegmatis (P407/Ms-IL15). The P407/Ms-IL15 system undergoes a sol-gel transformation at physiological temperatures, enhancing drug retention and diffusion while prolonging its duration of action. In an abdominal metastasis model,

intraperitoneal administration of P407/Ms-IL15 facilitated local drug retention and significantly enhanced anti-tumor efficacy. Local injection of P407/Ms-IL15 notably promoted dendritic cell (DC) maturation, increased the proportions of T cells and GZMB, and reduced M2 macrophage polarization. Furthermore, P407/Ms-IL15 demonstrated excellent biocompatibility both in vivo and in vitro, providing a safe and promising strategy for the treatment of abdominal metastases.

Supplementary Information

The online version contains supplementary material available at <https://doi.org/10.1186/s12967-025-06454-x>.

Supplementary Material 1

Acknowledgements

We thank all members of the Clinical Cancer Institute of Nanjing University for their discussion and suggestions during the period of this study.

Author contributions

Qi Wang: Writing—original draft, Visualization, Validation, Methodology, Data curation and conceptualization. Yi Mei: Visualization, Validation. Wenmei Rao: Validation. Sen Hong: Investigation. Aoxing Chen: Investigation, Formal analysis. Yang Yang: Supervision, Methodology. Qin Liu: Writing—review & editing, Supervision, Methodology, Funding acquisition, Conceptualization.

Funding

This study was supported by the Jiangsu Province “333” project (grant No. (2022)3-1-234).

Data availability

The data that support the findings of this study are available from the corresponding author upon reasonable request.

Declarations

Ethics approval and consent to participate

All animal experiments were approved by the Laboratory Animal Care and Use Committee of the Affiliated Nanjing Drum Tower Hospital of Nanjing University Medical School (Checking number: 2023AE01066), and were carried out in compliance with all relevant ethical regulations.

Consent for publication

Not applicable.

Competing interests

The authors declare that they have no known competing financial interests or personal relationships that could have appeared to influence the work reported in this paper.

Author details

¹Department of Oncology, Nanjing Drum Tower Hospital, Clinical College of Nanjing Drum Tower Hospital, Nanjing University of Chinese Medicine, 321 Zhongshan Road, Nanjing 210008, China

²Department of Oncology, Nanjing Drum Tower Hospital Group Suqian Hospital, The Affiliated Suqian Hospital of Xuzhou Medical University, Suqian, Jiangsu, China

³Department of Oncology, Nanjing Drum Tower Hospital, Affiliated Hospital of Medical School, School of Life Sciences, Nanjing University, Nanjing, China

⁴The Comprehensive Cancer Center, Nanjing Drum Tower Hospital, Affiliated Hospital of Medical School, Nanjing University, 321 Zhongshan Road, Nanjing 210008, China

⁵Department of Oncology, Nanjing Drum Tower Hospital, Clinical College of Nanjing Drum Tower Hospital, Nanjing University of Chinese Medicine, Nanjing, China

Received: 21 December 2024 / Accepted: 2 April 2025

Published online: 06 May 2025

References

1. Baaten ICPA, West NP, Quyn AJ, Seymour MT, Seligmann JF. Colorectal cancer peritoneal metastases: biology, treatment and next steps. *Eur J Surg Oncol*. 2020;46:675–83.
2. Yuan Z, Xu T, Cai J, Zhao Y, Cao W, Fichera A, et al. Development and validation of an Image-based deep learning algorithm for detection of synchronous peritoneal carcinomatosis in colorectal cancer. *Ann Surg*. 2022;275:e645–51.
3. Muro K, Boku N, Shimada Y, Tsuji A, Sameshima S, Baba H, et al. Irinotecan plus S-1 (IRIS) versus fluorouracil and folinic acid plus Irinotecan (FOLFIRI) as second-line chemotherapy for metastatic colorectal cancer: a randomised phase 2/3 non-inferiority study (FIRIS study). *Lancet Oncol*. 2010;11:853–60.
4. Boku N, Yamamoto S, Fukuda H, Shirao K, Doi T, Sawaki A, et al. Fluorouracil versus combination of Irinotecan plus cisplatin versus S-1 in metastatic gastric cancer: a randomised phase 3 study. *Lancet Oncol*. 2009;10:1063–9.
5. Ishigami H, Fujiwara Y, Fukushima R, Nashimoto A, Yabusaki H, Imano M, et al. Phase III trial comparing intraperitoneal and intravenous Paclitaxel plus S-1 versus cisplatin plus S-1 in patients with gastric cancer with peritoneal metastasis: PHOENIX-GC trial. *J Clin Oncol*. 2018;36:1922–9.
6. De Visser KE, Joyce JA. The evolving tumor microenvironment: from cancer initiation to metastatic outgrowth. *Cancer Cell*. 2023;41:374–403.
7. Young SL, Murphy M, Zhu XW, Harnden P, O'Donnell MA, James K, et al. Cytokine-modified *Mycobacterium smegmatis* as a novel anticancer immunotherapy. *Int J Cancer*. 2004;112:653–60.
8. Rich FJ, Kuhn S, Hyde EJ, Harper JL, Ronchese F, Kirman JR. Induction of T cell responses and recruitment of an inflammatory dendritic cell subset following tumor immunotherapy with *Mycobacterium smegmatis*. *Cancer Immunol Immunother*. 2012;61:2333–42.
9. Jeong H, Lee S-Y, Seo H, Kim B-J. Recombinant *Mycobacterium smegmatis* delivering a fusion protein of human macrophage migration inhibitory factor (MIF) and IL-7 exerts an anticancer effect by inducing an immune response against MIF in a tumor-bearing mouse model. *J Immunother Cancer*. 2021;9:e003180.
10. Duong MT-Q, Qin Y, You S-H, Min J-J. Bacteria-cancer interactions: bacteria-based cancer therapy. *Exp Mol Med*. 2019;51:1–15.
11. Zhou Y, Husman T, Cen X, Tsao T, Brown J, Bajpai A, et al. Interleukin 15 in Cell-Based cancer immunotherapy. *Int J Mol Sci*. 2022;23:7311.
12. Charbonneau MR, Isabella VM, Li N, Kurtz CB. Developing a new class of engineered live bacterial therapeutics to treat human diseases. *Nat Commun*. 2020;11:1738.
13. Thambi T, Li Y, Lee DS. Injectable hydrogels for sustained release of therapeutic agents. *J Controlled Release*. 2017;267:57–66.
14. Boonlai W, Tantishaiyakul V, Hirun N, Sangfai T, Suknuntha K. Thermosensitive poloxamer 407/Poly(Acrylic Acid) Hydrogels with Potential Application as Injectable Drug Delivery System. *AAPS PharmSciTech*. 2018;19:2103–17.
15. Chung CK, Fransen MF, Van Der Maaden K, Campos Y, García-Couce J, Kralisch D, et al. Thermosensitive hydrogels as sustained drug delivery system for CTLA-4 checkpoint blocking antibodies. *J Controlled Release*. 2020;323:1–11.
16. Chen A. Injectable thermo-sensitive hydrogel enhances anti-tumor potency of engineered *Lactococcus lactis* by activating dendritic cells and effective memory T cells. *Bioact Mater*. 2024.
17. Meng J, Yang X, Huang J, Tuo Z, Hu Y, Liao Z, et al. Ferroptosis-Enhanced immunotherapy with an injectable Dextran-Chitosan hydrogel for the treatment of malignant Ascites in hepatocellular carcinoma. *Adv Sci*. 2023;10:2300517.
18. Chen C, Li Z, Xiong X, Yao A, Wang S, Liu X, et al. Intraperitoneal PD-1 monoclonal antibody for the treatment of advanced primary liver cancer with malignant ascites: a single-arm, single-center, phase Ib trial. *ESMO Open*. 2024;9:102206.
19. Guo C, Liu J, Zhang Y. Current advances in bacteria-based cancer immunotherapy. *Eur J Immunol*. 2024;54:2350778.

20. Zhou M, Tang Y, Xu W, Hao X, Li Y, Huang S, et al. Bacteria-based immunotherapy for cancer: a systematic review of preclinical studies. *Front Immunol.* 2023;14:1140463.
21. Van Puffelen JH, Keating ST, Oosterwijk E, Van Der Heijden AG, Netea MG, Joosten LAB, et al. Trained immunity as a molecular mechanism for BCG immunotherapy in bladder cancer. *Nat Rev Urol.* 2020;17:513–25.
22. Yarkoni E, Rapp HJ. Immunotherapy of experimental cancer by intralesional injection of emulsified nonliving mycobacteria: comparison of *Mycobacterium Bovis* (BCG), *Mycobacterium Phlei*, and *Mycobacterium smegmatis*. *INFECT IMMUN.* 1980;28.
23. Cheadle EJ, O'Donnell D, Selby PJ, Jackson AM. Closely related mycobacterial strains demonstrate contrasting levels of efficacy as antitumor vaccines and are processed for major histocompatibility complex class I presentation by multiple routes in dendritic cells. *INFECT IMMUN.* 2005;73.
24. Jian W, Li X, Kang J, Lei Y, Bai Y, Xue Y. Antitumor effect of Recombinant *Mycobacterium smegmatis* expressing MAGEA3 and SSX2 fusion proteins. *Exp Ther Med.* 2018.
25. Aghlara-Fotovat S, Musteata E, Doerfert MD, Baruch M, Levitan M, Tabor JJ, et al. Hydrogel-encapsulation to enhance bacterial diagnosis of colon inflammation. *Biomaterials.* 2023;301:122246.
26. Yang Z, Zhu Y, Dong Z, Hao Y, Wang C, Li Q, et al. Engineering bioluminescent bacteria to boost photodynamic therapy and systemic anti-tumor immunity for synergistic cancer treatment. *Biomaterials.* 2022;281:121332.
27. Zhang Y, Kang R, Zhang X, Pang G, Li L, Han C, et al. A programmable oral bacterial hydrogel for controllable production and release of nanovaccine for tumor immunotherapy. *Biomaterials.* 2023;299:122147.
28. Li C, Nyaruaba R, Zhao X, Xue H, Li Y, Yang H, et al. Thermosensitive hydrogel wound dressing loaded with bacteriophage lysin LysP53. *Viruses.* 2022;14:1956.
29. Moskovicz V, Ben-El R, Horev G, Mizrahi B. Skin microbiota dynamics following *B. subtilis* formulation challenge: an in vivo study in mice. *BMC Microbiol.* 2021;21:231.

Publisher's note

Springer Nature remains neutral with regard to jurisdictional claims in published maps and institutional affiliations.